Review article

Nuclear Medicine Communications

Practical guidelines for the use of technetium-99m mebrofenin hepatobiliary scintigraphy in the quantitative assessment of liver function

Fadi Rassam[a], Pim B. Olthof[a], Hamish Richardson[c], Thomas M. van Gulik[a] and Roelof J. Bennink[b]

Surgical resection remains the most important curative treatment for liver tumors; however, it harbors the risk of developing posthepatectomy liver failure. The principal risk is associated with the quality and quantity of the future remnant liver. Therefore, preoperative assessment of the future remnant liver is essential in patients scheduled for major liver resection. Technetium-99m mebrofenin hepatobiliary scintigraphy (HBS) in combination with single-photon emission computed tomography/computed tomography is increasingly applied for the quantitative assessment of liver function before major liver surgery. This dynamic quantitative liver function test allows assessment of both total and regional liver function, represented by the hepatic mebrofenin uptake rate, thereby assisting in adequate patient selection. Since routine implementation, it has shown to reduce the risk of posthepatectomy liver failure and has proven to be more valuable than volumetric assessment. To ensure optimal and reproducible results that can be compared across different centers, it is crucial to standardize the methodology and ensure practical applicability of this technique, thereby facilitating external validation and multicenter trials. This article provides an overview of the HBS methodology used at some of the largest HBS centers and covers practical details in the application of HBS for the quantitative scintigraphic assessment of liver function. ***Nucl Med Commun*** **40:297–307**

Nuclear Medicine Communications 2019, **40**:297–307

Keywords: hepatobiliary scintigraphy, liver function, methodology, standardization

Departments of [a]Surgery, [b]Radiology and Nuclear Medicine, Cancer Center Amsterdam, Amsterdam UMC, University of Amsterdam, The Netherlands and [c]Department of Nuclear Medicine, Western General Hospital, Edinburgh, UK

Correspondence to Fadi Rassam, MD, Department of Surgery, Amsterdam UMC, University of Amsterdam, Meibergdreef 9, Amsterdam 1105 AZ, The Netherlands Tel: +31 205 665 568; fax: +31 206 976 621; e-mail: f.rassam@amc.uva.nl

Received 25 October 2018 **Revised** 9 December 2018
Accepted 15 December 2018

Introduction

Major liver resection can be performed with limited morbidity and mortality when sufficient remnant liver remains to avoid posthepatectomy liver failure (PHLF) [1,2]. To prevent the development of PHLF, sufficient functioning liver tissue must remain to uphold metabolic functions and homeostasis. Preoperative assessment of the future remnant liver (FRL) is therefore essential in patients scheduled for major liver resection. Traditionally, computed tomography (CT)-volumetric assessment was the standard method to evaluate the remnant liver; however, this does not necessarily reflect liver function, and therefore quantitative functional tests are gaining interest [3–5].

Different modalities have been used to measure liver function, varying from simple blood tests (e.g. bilirubin and prothrombin time) and clinical grading systems (e.g. Child–Pugh or Model for End-Stage Liver Disease scoring systems) to dynamic quantitative liver function tests like indocyanine green clearance test and scintigraphy tests [6–9]. Most of these methods are merely an indirect measure of actual liver function and only quantify the overall liver function. Technetium-99m (^{99m}Tc) mebrofenin hepatobiliary scintigraphy (HBS) in combination with single-photon emission computed tomography/computed tomography (SPECT-CT) is increasingly applied for the quantitative assessment of the total and regional liver function before major liver surgery. This method allows assessment of specifically, remnant liver function, defined as the mebrofenin uptake rate (MUR) and can also provide additional data on mebrofenin excretion.

HBS for the assessment of FRL function has been routinely used in Amsterdam since 2010. However, the indications, methodology, and interpretation have continued to evolve [10]. Moreover, in the absence of uniform commercially available processing software, several departments across the globe have been working with different acquisition methods and unautomated or semiautomated analysis algorithms, resulting in different outcome values and methods [11–13]. To ensure optimal and reproducible results that can be compared across different centers, it is crucial to standardize the methodology and practical applicability of this technique, thereby enabling external validation and multicenter trials.

This report aims to provide an overview of the HBS methodology incorporating the Ekman algorithm [14]

DOI: 10.1097/MNM.0000000000000973

used at some of the largest HBS centers and to cover practical details in the application of HBS for quantitative scintigraphic assessment of liver function.

Standardized method for the assessment of liver function using technetium-99m mebrofenin hepatobiliary scintigraphy

Radiopharmaceutical

Iminodiacetic acid (IDA) agents were developed by Loberg *et al.* [15]. These lidocaine analogues have lipophilic properties and are taken up by hepatocytes and eliminated through the bile. They provide means to examine the hepatobiliary system, in particular for the diagnosis of various biliary diseases [16,17]. They are bound to albumin and transported to the liver, which is the main organ of uptake. IDA agents do not undergo metabolization and share the same metabolic pathways with a number of endogenous and exogenous substances (such as bilirubin, toxins, and hormones), making them ideal agents to represent important functions of the liver [18,19].

Of all IDA analogues, mebrofenin (2,4,6 trimethyl-3-bromoiminodiacetic acid) shows the highest hepatic uptake and minimal urinary excretion [20,21]. The hepatic uptake is mediated by organic anion transporter polypeptides 1B1 and 1B3 and the biliary excretion by multidrug resistant protein 2 [18,22]. Elevated plasma bilirubin can affect the hepatic uptake of mebrofenin owing to competitive uptake at the organic anion transporter polypeptide receptors; likewise, hypoalbuminemia can decrease the hepatic delivery of mebrofenin as albumin is its main plasma carrier [23]. Of all IDA analogues, mebrofenin shows the highest resistance to the competitive uptake caused by elevated serum bilirubin [20].

^{99m}Tc-mebrofenin has to be prepared, preferably in-house, using a commercial kit, just before intravenous administration. The adult dose is 200 MBq enabling fast dynamic and SPECT acquisition with enough information to allow for pixel-based dynamic geometric mean (G_{mean}) and iterative SPECT reconstruction.

The administration of ^{99m}Tc-mebrofenin should be as close to the time of preparation as possible, preferably within 1 h. This is to prevent radiopharmaceutical degradation; longer labeling to administration time could lead to potential underestimation of the liver function [24].

The radiopharmaceutical is injected as a bolus through an intravenous line in an antecubital vein, followed by a 10-ml saline flush. The arm is extended to prevent stasis or slow release into the systemic circulation. This can result in a delayed delivery of the radiopharmaceutical to the systemic circulation, which consequently can underestimate the hepatic uptake.

Patient preparation

Patient preparation is crucial in the reproducibility of the results. The kinetics of mebrofenin uptake in the liver are influenced by blood flow, biliary excretion, and gastrointestinal motility (including the gallbladder). Patients are required to fast 4 h before the scan, for reasons of standardization. Prolonged fasting for a period longer than 24 h is undesirable as it can cause alteration in biliary kinetics [25]. Another factor that could be of importance is the use of some medications, like opioids, that act on the mysenteric plexus reducing gut motility.

Positioning

The patient is positioned supine on a dual opposing head γ-camera with low-energy high-resolution collimated detectors in an anterior and posterior patient position. The field of view (FOV) must include the heart, liver, and biliary area. In practice, the suprasternal notch ('angle of Louis') and the navel are used as landmarks for the superior and inferior edges within the FOV. The arm of the patient is extended perpendicular to the body and elevated at 25°–30° to prevent venous retention of the injected activity. As calculation of the hepatic uptake of mebrofenin start 150 s after injection, it is still possible to reposition the patient during the first 2 min if necessary so that the camera covers the required FOV. As the SPECT scan has to start as soon as possible after the first dynamic phase, the arms are positioned above the head immediately after injection of the radiopharmaceutical.

Acquisition

First phase: dynamic: hepatic uptake

Immediately after the intravenous bolus injection of the radiopharmaceutical, the dynamic acquisition is started. A total of 38 frames of 10 s/frame are taken using a 128×128 matrix size. At least 36 frames (6 min) are needed for the calculation of the hepatic uptake rate. Two additional frames are made to enable compensation for eventual early acquisition start or delayed systemic bolus arrival. The detectors of the γ-camera are aligned, as required by the quality criteria parameters. In this early phase, the tracer travels through the circulation and is taken up by the hepatocytes. At the end of this phase, most of the tracer is accumulated in the liver.

Second phase: single-photon emission computed tomography/computed tomography

During the study, the tracer is taken up by the hepatocytes and is gradually excreted in the biliary system. Immediately after the first dynamic acquisition, a SPECT is acquired. This takes place in the phase in which the highest amount of the tracer is accumulated in the liver and before enhanced excretion into the bile ducts, making it possible to depict the three-dimensional distribution of the radioactivity in the liver at its peak uptake [26].

The acquisition is performed for 60 frames with 8 s/frame using a 256×256 matrix using a low-energy high-resolution collimator. The FOV is identical to the first phase acquisition. Subsequently, a low-dose non-contrast-enhanced CT (CT_{low}

20 mA, 110 kV) is obtained. This is done without moving the patient to make fusion possible. In general, it is not advised to use breath holding techniques for the attenuation correction CT, as this tends to generate more mismatch artifacts. The CT_{low} is only used for anatomical mapping and attenuation correction.

Third phase: dynamic: excretion phase

Finally, a second dynamic acquisition, 20 frames of 60 s/frame using a 128×128 matrix is acquired to establish biliary excretion and evaluate the presence and potential effect of biliary obstruction. The FOV is identical to the first phase acquisition.

Processing

Visual assessment

Dynamic images can be viewed in cine mode or reformatted into 20 or 30 s frames for visual inspection of movement and biodistribution. Normal findings are characterized by the immediate demonstration of hepatic uptake and rapid clearance of cardiac pool activity, without projection of the heart region over the hepatic area. The images are evaluated for persistence of blood pool (BP) activity and hepatic uptake. A focal blush can signal a lesion with arterial hypervascularization (prominent in hepatocellular carcinoma, adenoma, and focal nodular hyperplasia) just before the portal phase. Conversely, decreased flow can be seen in hypovascular lesions (e.g. large metastases and abscess of cystic lesions) [27]. On delayed imaging (excretion phase) activity in the biliary ductal system, gallbladder and/or upper small bowel will be visible or absent in case of biliary obstruction (Fig. 1).

In case of movement artefacts exceeding normal breathing variation, a motion correction should be applied. This can be performed manually by selecting the series of frames, or automatically if supported by the available software package.

If sustained activity throughout the route of administration and/or subclavian vein is present during the first dynamic images, this can be masked and removed manually as the calculations are based on relative corrected activity.

Global liver function: mebrofenin uptake rate

First, the ^{99m}Tc-MUR (%/min) is calculated, and this corresponds with the total liver uptake and reflects global liver function. This is based on the whole field of view and liver activity, allowing for calculation of the relative uptake rate as outlined in the original Ekman formula [28].

To compensate for the attenuation caused by the depth difference on both sides of the liver (where the left segments lie more anteriorly and the right segments posteriorly), a geometric mean (G_{mean}) dataset is generated. The G_{mean} is obtained from the anterior and posterior dynamic acquisitions from which the square root of their product is calculated ($\sqrt{\text{anterior} \times \text{posterior}}$) and projected in anterior view. This method provides a more accurate estimation compared with calculating the uptake on both anterior and posterior data sets separately. Moreover, the heart is highly attenuated in the posterior acquisition, and if the data sets are used separately, it will lead to a strong decline of counts in the BP and therefore, providing a poor estimation in the posterior data set.

Depending on the software that is used, the G_{mean} can be calculated either on pixel-by-pixel base or ROI based. In pixel-by-pixel basis, the G_{mean} values between each pixel pair that corresponds to the same position in the image set are calculated. The caveat of this method is that whenever in one of the views a pixel would have a zero count whereas not in the other view, the result of the G_{mean} value of that particular pixel will be zero. However, using sufficient radiopharmaceutical and appropriate collimation circumvents this issue. If G_{mean} calculation is based on ROI analysis, the total counts in anterior and posterior images are summed leading to homogenization of function, potentially inducing error in assessment of true regional function.

The newly generated G_{mean} data set is further analyzed to calculate the MUR. A timeframe is chosen that falls between the homogenous distribution of the tracer in the BP and extraction in the bile canaliculi. This is generally between 150 and 350 s. The frame where the abdominal aorta is primarily visible is considered as a landmark for the first frame, and any earlier frames are discarded. This ensures equal time frames in all patients because the starting time point of the acquisition after intravenous bolus may slightly differ per technologist or subject. Therefore, two additional frames are taken during the first phase allowing the possibility to correct for early acquisition or delayed bolus arrival in the circulation.

Time–activity curves are then generated based on defined regions of interest (ROI). Three ROIs are drawn around the liver, the left ventricle including the aortic root corresponding with the BP, and around the total FOV, indicative of the total body activity.

The liver ROI is drawn on a summed image of 20 consecutive frames starting from the 16th frame. There should be a smooth delineation where the entire organ is included in the ROI extending at least one pixel outside the liver edges [29].

The BP ROI is drawn on the first frames of the dynamic set. For this ROI, it is important not to draw too small or too large. It should include the left ventricle and extend to the aortic root. Extending the ROI outside the cardiac chambers would dramatically lower the total BP counts because of the significantly lower count density outside the left ventricle. Furthermore, it is important that the BP ROI is positioned at some distance from the liver to ensure minimal contribution from the scattered liver activity. A check is done to ensure that there is no overlap between the liver activity and the BP ROI within the

Fig. 1

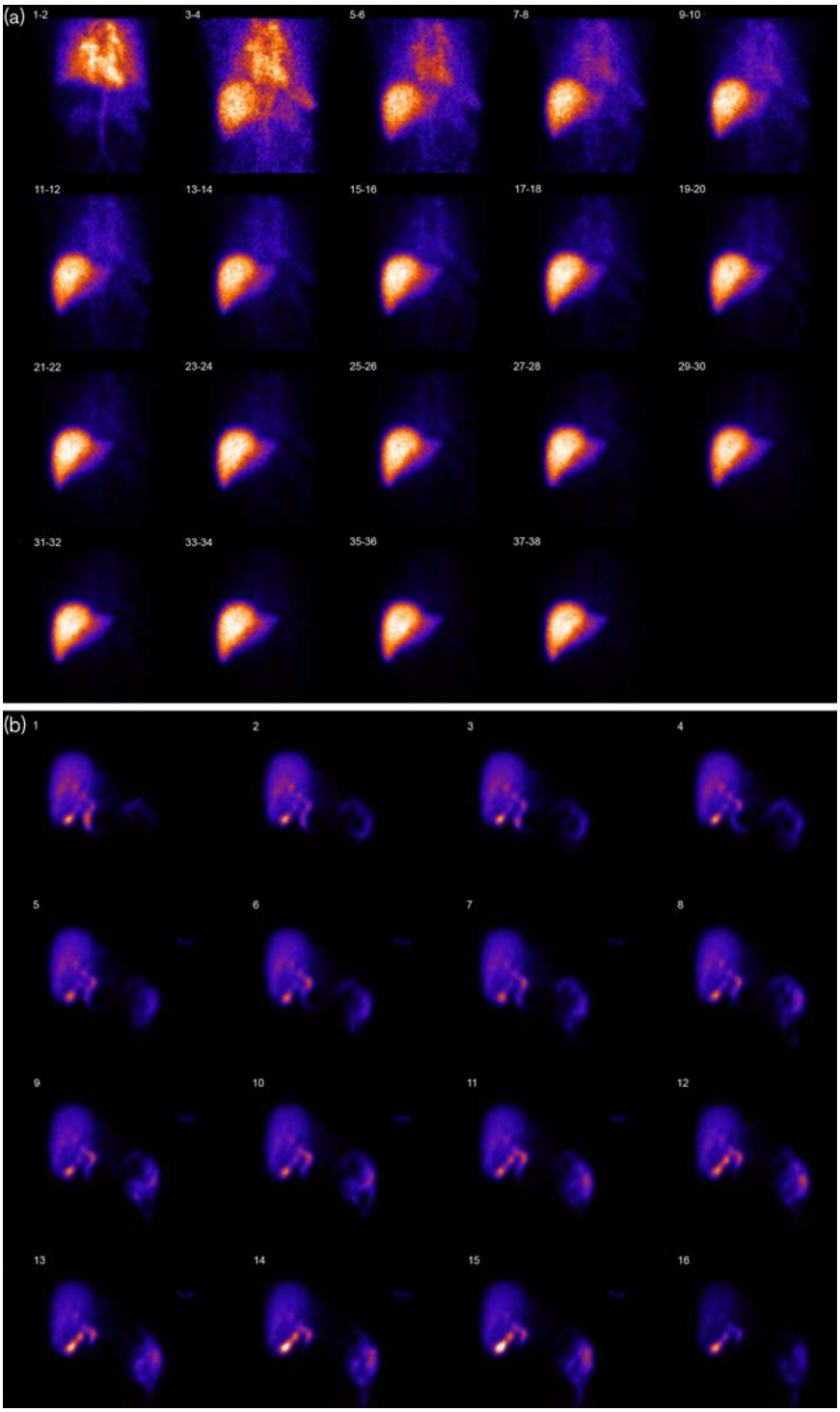

Early (a) and late (b) dynamic phases showing normal hepatic uptake, blood clearance, and biliary excretion.

frames that contribute to the liver uptake calculations (frames 16–36). In case of overlap, the BP ROI should be adjusted.

Finally, a third ROI is drawn that encompasses all counts on the frame. Depending on the software package used, this can be automated (Fig. 2).

With these three time–activity curves, the hepatic uptake is calculated as described by Ekman *et al.* [14]. Here it is assumed that between 150 and 350 s, the tracer is distributed evenly in the BP. In this case, the use of a monoexponential fit gives a good model of the concentration of circulating activity. As frames are 10 s each, and counts per frame are the sum of all events within the 10-s period, the counts at t of 150 and 350 s have to be determined by processing as follows:

$$\text{Counts } t_{150} = \frac{\text{Counts frame 15} + \text{counts frame 16}}{2}.$$

$$\text{Counts } t_{350} = \frac{\text{Counts frame 35} + \text{counts frame 36}}{2}.$$

The MUR is presented as percentage of total administered ^{99m}Tc-mebrofenin activity accredited by liver per minute.

Fig. 2

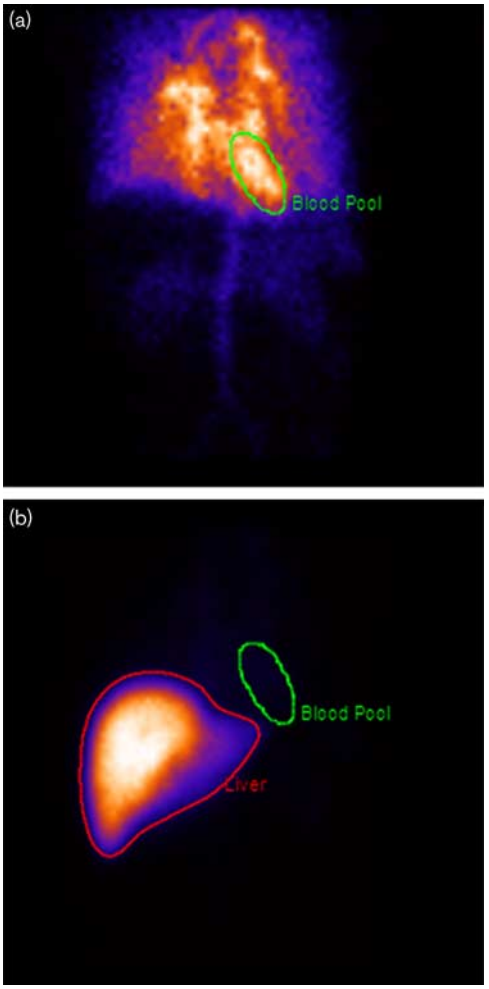

Region of interest (ROI) on early phase: blood pool ROI is drawn on the first one or two (summed) frames (a), and the liver ROI on summed image of 20 consecutive frames starting from the 16th frame (b).

To compensate for individual differences in metabolic requirements, the MUR is divided by the body surface area, which can be calculated by the Mosteller formula [30]. The resulting liver function is the corrected MUR (cMUR), expressed as %/min/m^2.

Functional distribution

The cMUR only provides information on global liver function. The SPECT acquisition provides a three-dimensional functional distribution that can be used to calculate the functional share, or the functional volume, of the FRL. As mentioned before, this is crucial for determination of the FRL function as the functional distribution does not correspond with the volumetric share in all patients [10]. The SPECT acquisition is performed immediately after the first dynamic phase, in a period of relatively stable mebrofenin uptake. This is combined with a low-dose CT that is used for attenuation correction and anatomical mapping. Attenuation correction compensates for the decline of activity because of the absorption of γ-rays in the deep, centrally located liver parenchyma.

The timing of the SPECT is challenging. Ideally, it is centered at the peak of the hepatic activity when the amount of radioactivity is most stable within the hepatocytes. In patients with a fast hepatic uptake, the SPECT will extend into the excretion phase. If the accumulation of radioactivity in the intrahepatic or extrahepatic bile ducts is visible on SPECT, the relatively high pixel values are not representative for hepatocellular uptake and will disturb threshold-based calculations. In this case, the external bile ducts (including hilar activity) are removed using a masking tool. The radioactivity within the intrahepatic bile ducts is replaced by average counts of the adjacent liver parenchyma, assuming that the volume of intrahepatic biliary structures is virtually negligible (enlarged bile ducts because of biliary obstruction should be decompressed before HBS). A small, representative region of normal liver tissue without biliary structures is selected to measure the average voxel counts, and this value is used to replace the radioactivity within the intrahepatic bile ducts. A problem with livers that have diffuse intrahepatic biliary stasis is that too much masking can lead to homogenization of the liver. Therefore, one always has to consider the benefit and potential hazard of the corrective intervention.

The bile ducts can be outlined manually on each separate slice or summed sequential slices. Modern software offers the possibility to outline the bile ducts in a semiautomated manner using a volume-of-interest masking tool. The masking is an iterative process where insufficient bile duct masking or excessive masking of normal liver tissue should be avoided. Insufficient bile duct masking will result in a rim of high activity on the edge of the biliary structures, whereas in excessive masking, too much normal liver tissue will be homogenized, leading to inaccurate results (Fig. 3).

After masking the bile ducts, the FRL is outlined on SPECT-CT to provide masks of the segments that are to be

Fig. 3

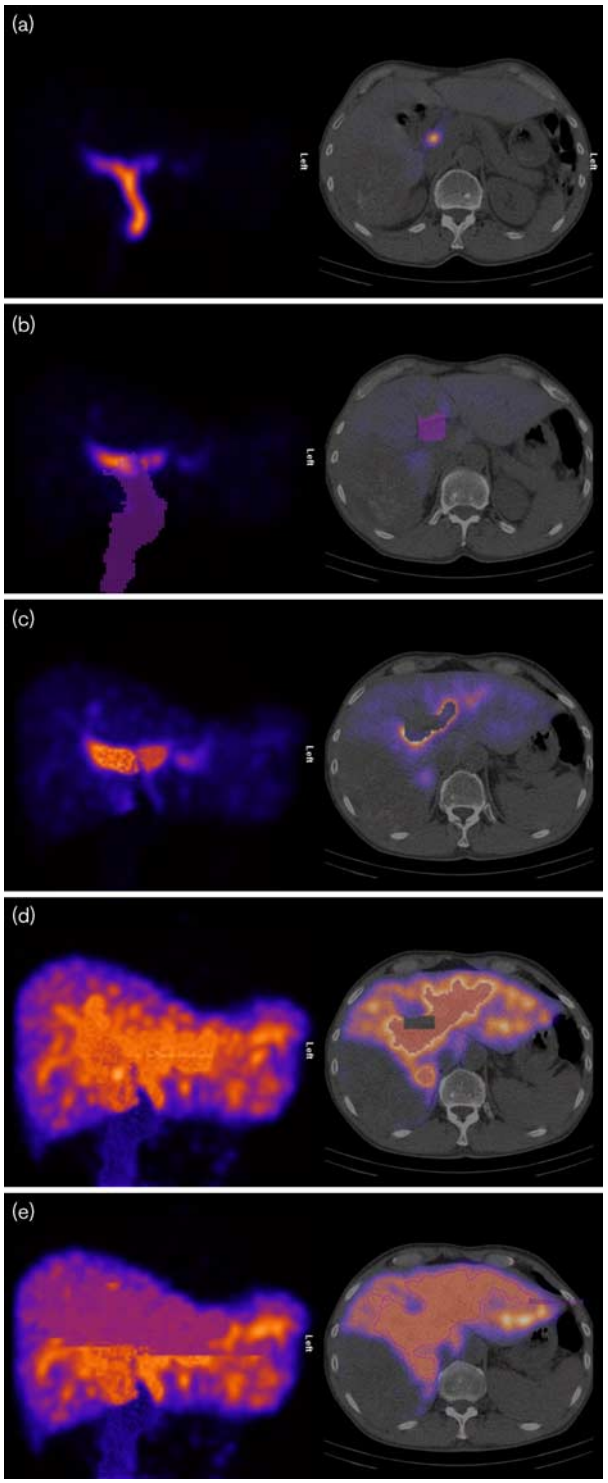

Single-photon emission computed tomography/computed tomography without (a), with insufficient (b, c), sufficient (d) or too much (e) masking of the bile ducts.

removed. For accurate segmental delineation, recent contrast-enhanced CT or MRI can be used whenever available for anatomical landmarks simultaneously with the CT_{low} for concurrent anatomical mapping. Moreover, it is often possible to see the segmental division of the liver on the functional images provided by SPECT. Fusion of SPECT with contrast-enhanced CT is hazardous as clinical protocols tend to use different breath-hold strategies. On inspiration, the liver not only moves in a craniocaudal direction but also rotates in the sagittal plane. Several landmarks are used to delineate the segments of the FRL according to Couinaud's functional segmentation of the liver; the Falciform ligament is used for the border between segments 2/3 and 4, the gallbladder and middle hepatic vein for the border between segments 4 and 5/8 (also known as Cantlie's line), and the right hepatic vein as the border between segments 5/8 and 6/7 (Fig. 4) [31–33].

An outline extraction model is used to calculate the counts of the total liver and the FRL. This is applied to automatically outline the liver and calculate the total functional liver volume. This calculation is threshold based in which in most cases, the threshold is set at 20–30% of the maximal voxel value.

The functional share is calculated as the ratio of the FRL counts to the total liver counts, expressed as a percentage of total liver function. To calculate the function of the FRL, the cMUR is multiplied by the functional share.

Hepatic excretion rate

The second 20-min dynamic acquisition, 20×1 min frames acquired immediately after the SPECT-CT, is used to calculate the biliary excretion rate. After generation of a G_{mean} data set, a ROI is drawn around a peripheral portion of the FRL. The excretion rate is calculated from the counts on the first and last frame and expressed in %/min using the following formula:

$$\text{Biliary excretion rate}\,(\%/\text{min}) = \frac{1 - \frac{\text{Counts ROI at frame 20}}{\text{Counts ROI at frame 1}}}{20} \times 100\,\%.$$

Normal values are greater than 0.5%/min. Excretion cannot be assessed in patients with very low cMUR.

Software packages

Several software packages are available on the market to process scintigraphic and SPECT-CT acquisitions. Hermes LiverRemnant (Hermes Medical Solutions, Stockholm, Sweden) and MIM (MIM Software Inc., Cleveland, Ohio, USA) are both capable of determining total and regional liver function and have been validated for the calculations of MUR using formulas for liver clearance based on the paper of Ekman *et al.* [28].

The software provides integrated workflow with which both the dynamic SPECT and CT acquisitions can be displayed and analyzed. G_{mean} is automatically calculated from the anterior and posterior dynamic data sets, and the hepatic uptake is calculated based on these data sets.

Fig. 4

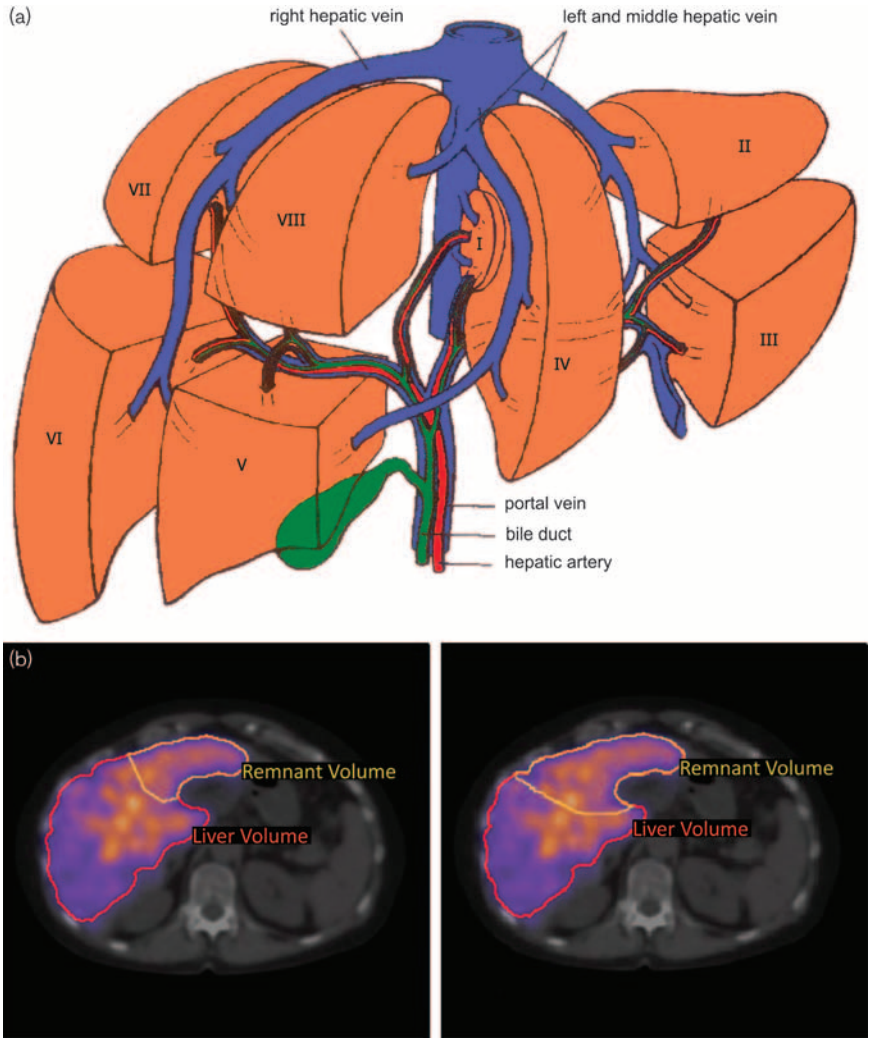

Couinaud segments of the liver (a) with segmentation S2–S3 versus S2–S4 on the fused SPECT and CT_{low} acquisitions (b). CT, computed tomography; SPECT, single-photon emission computed tomography.

The SPECT and CT images are fused and visible within the same workflow.

Dynamic data sets can be viewed in cine mode with variable slice adding for adequate visualization of tracer uptake and assessment of patient motion. The ROIs can be directly drawn on any frame. From the SPECT-CT series, masking of the biliary tree in a semiautomated manner with manual correction is supported, as well as manual delineation of FRL segments.

Clinical implications

It is expected that the incidence of primary and secondary hepatic tumors will continue to increase in the future, along with the demand for hepatic resections. At the same time, more complex resections are undertaken in patients with varying degrees of parenchymal damage following neoadjuvant regimens of systemic treatment. PHLF is one of the most serious complications after major liver resection. Many risk factors have been identified, which can be divided in patient related, surgery related, or related to postoperative care. The principal risk, however, is associated with the quality and quantity of the FRL [34]. Risk assessment is therefore of great importance to prevent the occurrence of PHLF.

CT volumetry has been the traditional method to assess resectability, using the volumetric share of the FRL as an indirect measure of liver function. With this modality, 25% of total liver volume is required in patients with normal liver parenchyma, whereas in patients with compromised liver parenchyma, at least 40% is required to undergo a safe resection [35,36]. A drawback of this method is that liver volume does not reflect liver function

per se [37]. Furthermore, liver function is not homogeneously distributed in the liver, especially in patients with compromised liver parenchyma or in patients who underwent liver-augmenting techniques like portal vein embolization (PVE) [5,10,38].

Quantitative assessment of liver function using nuclear imaging techniques offers the possibility to simultaneously provide both visual (anatomical) and functional information of the liver. The main advantage of HBS is that it can be used in patients with both normal and impaired liver parenchyma using the same cMUR cut-off value. The application of the current cutoff of 2.7%/min/m^2 has led to a significant decrease in PHLF [3]. To note, this cutoff was originally based on a mixed population of 55 patients with predominantly biliary tumors. Furthermore, at the time of determination of this value, only anterior projections were used for the dynamic acquisitions which can result in an underestimation of the right liver segments. Therefore, this cut-off value is at the higher end. Adherence to this cut-off value has led to a decrease in the incidence of PHLF but likely, also to a higher rate of patients deemed unresectable because of a FRLF below the threshold. This cutoff value can potentially differ depending on several patients' characteristics. For instance, patients with colorectal liver metastasis generally have healthy liver parenchyma with potentially more functional reserve capacity compared with patients with impaired liver parenchyma such as in patients with hepatocellular carcinoma and chronic liver disease or patients with biliary tumors and posthepatic obstruction leading to cholestasis. The first group probably can undergo safe resection with a lower cut-off value compared with the latter. Recently, the role of HBS was analyzed in 116 patients with perihilar cholangiocarcinoma, of which 27 developed PHLF [4]. The diagnostic value of MUR (%/min) and cMUR (%/min/m^2) was similar and a cut-off value for liver function was set at 8.5%/min, with a negative predictive value of 94%. Because of the decreased incidence of PHLF on the one hand and lack of uniformity to compare results across different centers on the other hand, it is difficult to conduct multicenter trials to validate new cutoff values. Therefore, standardization of HBS methodology is essential to pursue validation studies.

A caveat of HBS is that ^{99m}Tc-mebrofenin uptake is competitive with bilirubin as both are taken up by the same hepatocyte transporter systems [18]. This is of relevance in patients with hyperbilirubinemia, which is frequently present in patients with biliary tumors. In these patients, hepatocyte function is likely decreased which will be appropriately reflected by HBS, with even more underestimation because of competition (Fig. 5). Furthermore, biliary excretion, facilitated by multidrug resistance-associated protein 2 receptor, can also be impaired because of biliary obstruction caused by tumor growth. During hyperbilirubinemia, these receptors are downregulated, but their expression is gradually restored after biliary drainage [39,40]. Especially when bilirubin values exceed 50 μmol/l, outcome of cMUR is predictably (very) low, and application of HBS in the presence of obstructive cholestasis such as with biliary tumors should therefore be restricted to patients with adequate biliary drainage [4].

Neoadjuvant chemotherapy is given in patients with colorectal liver metastasis to downsize tumor burden. However, there are potential, chemotherapy-associated hepatotoxic effects that can reduce parenchymal quality and functional capacity of the FRL and consequently, resectability in terms of sufficient remnant liver. The influence of chemotherapy on liver function is temporary and potentially recovers after cessation [41,42].

Patients who are initially unresectable because of insufficient FRL function can benefit from techniques to increase FRL volume and function such as PVE or associating liver partition and portal vein ligation for staged hepatectomy (ALPPS). After PVE, it seems that the functional gain is more rapid and of greater magnitude than the volumetric increase [43]. This suggests that the waiting time after PVE can be reduced if function rather than volume is used to assess the hypertrophy response (Fig. 6).

Conversely in ALPPS, functional assessment early after stage 1 showed the increase in function of the FRL to be less pronounced than the volumetric increase [5,44]. This can in part explain the high complication rate after completion of ALPPS when CT volumetry is used for interstage assessment [45]. An explanation for this discrepancy after stage 1 is that the increase in volume is the result of proliferation of hepatocytes that are enlarged but have not yet undergone full maturation and therefore, stay behind in function [38,46]. The discrepancy between volume and function in the hypertrophy response further underscores the importance of functional assessment and the use of SPECT-CT to investigate the functional (segmental) distribution.

The biliary excretion phase can be useful for preoperative determination of segmental cholestasis and to check whether adequate drainage has been achieved. It has further utility in postoperative patients to assess biliary complications, such as bile leakage. However, the interference with bilirubin is also of relevance after surgery, for instance in case of high plasma bilirubin because of biliary complications or liver dysfunction. Application of HBS in these settings will not differentiate between low or adequate liver function. This might especially affect clinical decision making within the ALPPS procedure.

Several centers have modified calculations for FRL function using a combination of HBS parameters and CT volumetry. One group calculates FLR function by multiplying total liver function measured with HBS by the

Fig. 5

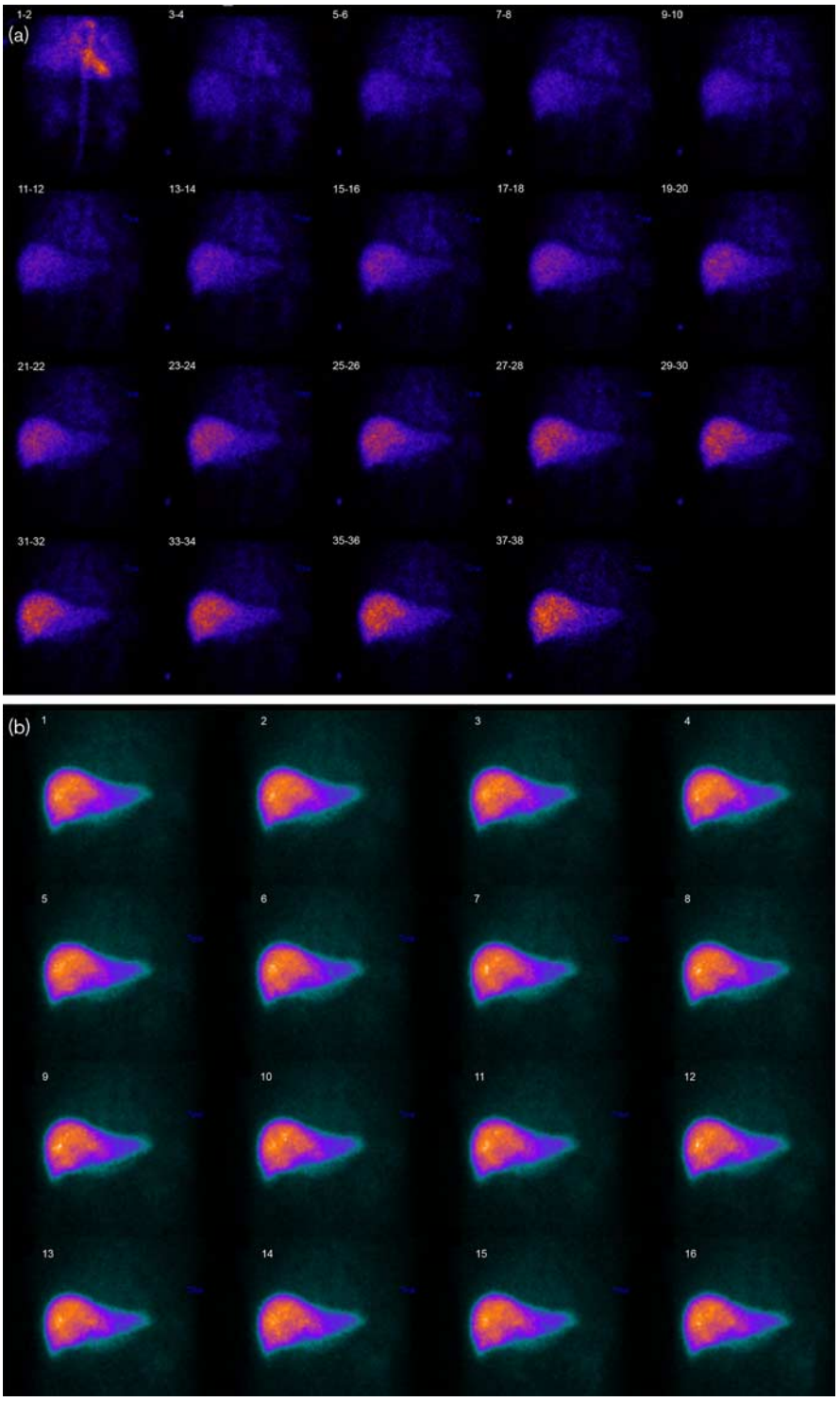

Dynamic phase in a patient with hyperbilirubinemia with serum bilirubin of 69 mmol/l. There is delayed hepatic uptake and clearance of mebrofenin from the blood pool (a). At the end of the early phase, the uptake has not been completed (a). During the late phase, there is no excretion visible to the bile ducts (b).

Fig. 6

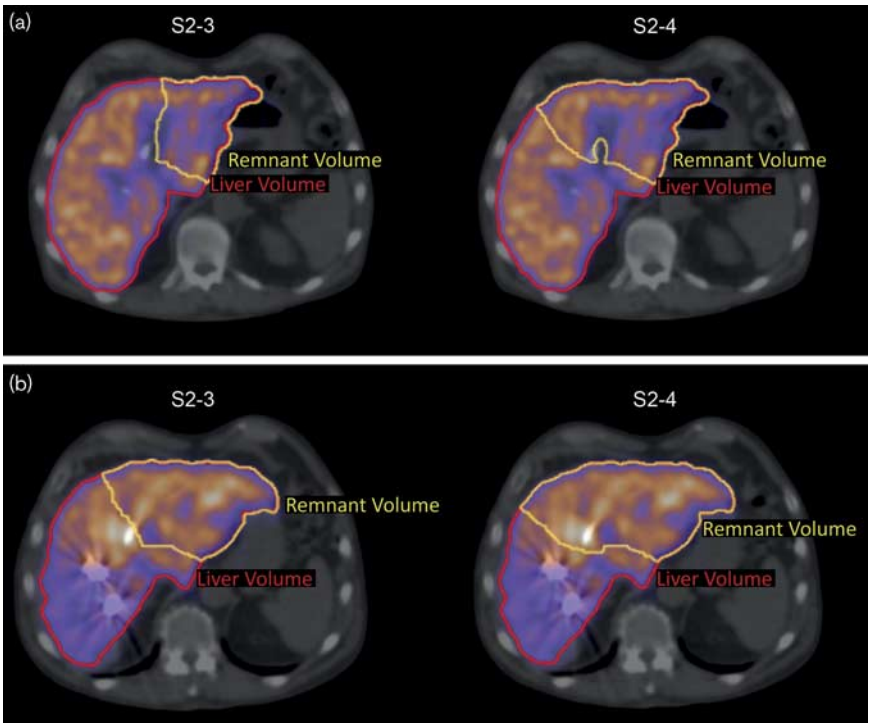

Segments 2–3 and 2–4 before (a) and after portal vein embolization (b).

share of FLR volume and demonstrated superior predictive value for PHLF using this parameter over FLR volume share alone [13]. As mentioned before, the assumption that liver function is homogenously distributed throughout the liver is not always valid [10]. By using the volume share, calculation of FLR function might be incorrect compared with the FLR functional share calculated using SPECT.

A group in Buenos Aires developed a new dynamic measure, the HIBA index, representing the proportion of radionuclide accumulation in the FRL [11]. This was obtained by calculating the area under the time–activity curve of the total liver (corrected for BP and total FOV) multiplied by the functional share calculated by SPECT [11]. Although promising, this was shown in only a small series of 20 patients for interstage assessment during the ALPPS procedure in a highly experienced center in which only four patients developed PHLF. Hence, several methods have been applied to calculate function of the FRL using HBS. To utilize these methods for optimal patient selection, there is a need for multicenter validation of HBS parameters and their cut-off values.

Conclusion

HBS provides information on total and regional (i.e. segmental) liver function. It is advised in any patient undergoing major liver resection as it can reduce the risk of PHLF and has proven to be more valuable than volumetric assessment. Furthermore, it has an important role in interstage assessment after liver-augmenting techniques like PVE and ALPPS, in view of the discrepancy between volume and function after these interventions. To validate the cutoff values and investigate its further clinical applicability, comparable and reproducible results have to be achieved to collect sufficient data among centers. The single most important step to reach that goal is to standardize the methodology and practical application of this technique.

Acknowledgements

Conflicts of interest

There are no conflicts of interest.

References

1 Agrawal S, Belghiti J. Oncologic resection for malignant tumors of the liver. *Ann Surg* 2011; **253**:656–665.
2 Jarnagin WR, Gonen M, Fong Y, DeMatteo RP, Ben-Porat L, Little S, *et al.* Improvement in perioperative outcome after hepatic resection: analysis of 1,803 consecutive cases over the past decade. *Ann Surg* 2002; **236**:397–406; (discussion 406–407).
3 Cieslak KP, Bennink RJ, de Graaf W, van Lienden KP, Besselink MG, Busch OR, *et al.* Measurement of liver function using hepatobiliary scintigraphy improves risk assessment in patients undergoing major liver resection. *HPB (Oxford)* 2016; **18**:773–780.
4 Olthof PB, Coelen RJS, Bennink RJ, Heger M, Lam MF, Besselink MG, *et al.* (99m)Tc-mebrofenin hepatobiliary scintigraphy predicts liver failure following major liver resection for perihilar cholangiocarcinoma. *HPB (Oxford)* 2017; **19**:850–858.

5 Olthof PB, Tomassini F, Huespe PE, Truant S, Pruvot FR, Troisi RI, *et al.* Hepatobiliary scintigraphy to evaluate liver function in associating liver partition and portal vein ligation for staged hepatectomy: liver volume overestimates liver function. *Surgery* 2017; **162**:775–783.
6 Schneider PD. Preoperative assessment of liver function. *Surg Clin North Am* 2004; **84**:355–373.
7 Kamath PS, Kim WR. Advanced Liver Disease Study Group. The model for end-stage liver disease (MELD). *Hepatology* 2007; **45**:797–805.
8 Lau H, Man K, Fan ST, Yu WC, Lo CM, Wong J. Evaluation of preoperative hepatic function in patients with hepatocellular carcinoma undergoing hepatectomy. *Br J Surg* 1997; **84**:1255–1259.
9 Kokudo N, Vera DR, Makuuchi M. Clinical application of TcGSA. *Nucl Med Biol* 2003; **30**:845–849.
10 de Graaf W, van Lienden KP, Dinant S, Roelofs JJ, Busch OR, Gouma DJ, *et al.* Assessment of future remnant liver function using hepatobiliary scintigraphy in patients undergoing major liver resection. *J Gastrointest Surg* 2010; **14**:369–378.
11 Serenari M, Collaud C, Alvarez FA, de Santibanes M, Giunta D, Pekolj J, *et al.* Interstage assessment of remnant liver function in ALPPS using hepatobiliary scintigraphy: prediction of posthepatectomy liver failure and introduction of the HIBA index. *Ann Surg* 2018; **267**:1141–1147.
12 Geisel D, Ludemann L, Froling V, Malinowski M, Stockmann M, Baron A, *et al.* Imaging-based evaluation of liver function: comparison of (9)(9)mTc-mebrofenin hepatobiliary scintigraphy and Gd-EOB-DTPA-enhanced MRI. *Eur Radiol* 2015; **25**:1384–1391.
13 Chapelle T, Op De Beeck B, Huyghe I, Francque S, Driessen A, Roeyen G, *et al.* Future remnant liver function estimated by combining liver volumetry on magnetic resonance imaging with total liver function on (99m)Tc-mebrofenin hepatobiliary scintigraphy: can this tool predict post-hepatectomy liver failure? *HPB (Oxford)* 2016; **18**:494–503.
14 Ekman M, Fjalling M, Holmberg S, Person H. IODIDA clearance rate: a method for measuring hepatocyte uptake function. *Transplant Proc* 1992; **24**:387–388.
15 Loberg MD, Cooper M, Harvey E, Callery P, Faith W. Development of new radiopharmaceuticals based on N-substitution of iminodiacetic acid. *J Nucl Med* 1976; **17**:633–638.
16 Krishnamurthy S, Krishnamurthy GT. Technetium-99m-iminodiacetic acid organic anions: review of biokinetics and clinical application in hepatology. *Hepatology* 1989; **9**:139–153.
17 Krishnamurthy GT, Turner FE. Pharmacokinetics and clinical application of technetium 99m-labeled hepatobiliary agents. *Semin Nucl Med* 1990; **20**:130–149.
18 de Graaf W, Hausler S, Heger M, van Ginhoven TM, van Cappellen G, Bennink RJ, *et al.* Transporters involved in the hepatic uptake of (99m) Tc-mebrofenin and indocyanine green. *J Hepatol* 2011; **54**:738–745.
19 Krishnamurthy GT, Krishnamurthy S. Cholescintigraphic measurement of liver function: how is it different from other methods? *Eur J Nucl Med Mol Imaging* 2006; **33**:1103–1106.
20 Nunn AD, Loberg MD, Conley RA. A structure–distribution–relationship approach leading to the development of Tc-99m mebrofenin: an improved cholescintigraphic agent. *J Nucl Med* 1983; **24**:423–430.
21 Chervu LR, Nunn AD, Loberg MD. Radiopharmaceuticals for hepatobiliary imaging. *Semin Nucl Med* 1982; **12**:5–17.
22 Ghibellini G, Leslie EM, Pollack GM, Brouwer KL. Use of Tc-99m mebrofenin as a clinical probe to assess altered hepatobiliary transport: integration of in vitro, pharmacokinetic modeling, and simulation studies. *Pharm Res* 2008; **25**:1851–1860.
23 Okuda H, Nunes R, Vallabhajosula S, Strashun A, Goldsmith SJ, Berk PD. Studies of the hepatocellular uptake of the hepatobiliary scintiscanning agent ^{99m}Tc-DISIDA. *J Hepatol* 1986; **3**:251–259.
24 Tulchinsky M, Allen TW. Longer Tc-99m-mebrofenin labeling-to-administration time results in scintigraphic underestimation of liver function. *Clin Nucl Med* 2011; **36**:1079–1085.
25 Tierney S, Pitt HA, Lillemoe KD. Physiology and pathophysiology of gallbladder motility. *Surg Clin North Am* 1993; **73**:1267–1290.
26 Oppenheim BE, Krepshaw JD. Dynamic hepatobiliary SPECT: a method for tomography of a changing radioactivity distribution. *J Nucl Med* 1988; **29**:98–102.
27 Yeh SH, Shih WJ, Liang JC. Intravenous radionuclide hepatography in the differential diagnosis of intrahepatic mass lesions. *J Nucl Med* 1973; **14**:565–567.
28 Ekman M, Fjalling M, Friman S, Carlson S, Volkmann R. Liver uptake function measured by IODIDA clearance rate in liver transplant patients and healthy volunteers. *Nucl Med Commun* 1996; **17**:235–242.
29 Tulchinsky M, Tun KN. Mebrofenin clearance rate for liver function testing: standardization of methodology aimed to improve intraobserver reproducibility. *Clin Nucl Med* 2012; **37**:644–648.
30 Mosteller RD. Simplified calculation of body-surface area. *N Engl J Med* 1987; **317**:1098.
31 Hata F, Hirata K, Murakami G, Mukaiya M. Identification of segments VI and VII of the liver based on the ramification patterns of the intrahepatic portal and hepatic veins. *Clin Anat* 1999; **12**:229–244.
32 van Leeuwen MS, Noordzij J, Fernandez MA, Hennipman A, Feldberg MA, Dillon EH. Portal venous and segmental anatomy of the right hemiliver: observations based on three-dimensional spiral CT renderings. *AJR Am J Roentgenol* 1994; **163**:1395–1404.
33 Rutkauskas S, Gedrimas V, Pundzius J, Barauskas G, Basevicius A. Clinical and anatomical basis for the classification of the structural parts of liver. *Medicina (Kaunas)* 2006; **42**:98–106.
34 Golse N, Bucur PO, Adam R, Castaing D, Sa Cunha A, Vibert E. New paradigms in post-hepatectomy liver failure. *J Gastrointest Surg* 2013; **17**:593–605.
35 Shoup M, Gonen M, D'Angelica M, Jarnagin WR, DeMatteo RP, Schwartz LH, *et al.* Volumetric analysis predicts hepatic dysfunction in patients undergoing major liver resection. *J Gastrointest Surg* 2003; **7**:325–330.
36 Kubota K, Makuuchi M, Kusaka K, Kobayashi T, Miki K, Hasegawa K, *et al.* Measurement of liver volume and hepatic functional reserve as a guide to decision-making in resectional surgery for hepatic tumors. *Hepatology* 1997; **26**:1176–1181.
37 Bennink RJ, Dinant S, Erdogan D, Heijnen BH, Straatsburg IH, van Vliet AK, *et al.* Preoperative assessment of postoperative remnant liver function using hepatobiliary scintigraphy. *J Nucl Med* 2004; **45**:965–971.
38 Matsuo K, Murakami T, Kawaguchi D, Hiroshima Y, Koda K, Yamazaki K, *et al.* Histologic features after surgery associating liver partition and portal vein ligation for staged hepatectomy versus those after hepatectomy with portal vein embolization. *Surgery* 2016; **159**:1289–1298.
39 Schaap FG, van der Gaag NA, Gouma DJ, Jansen PL. High expression of the bile salt-homeostatic hormone fibroblast growth factor 19 in the liver of patients with extrahepatic cholestasis. *Hepatology* 2009; **49**:1228–1235.
40 Keppler D. The roles of MRP2, MRP3, OATP1B1, and OATP1B3 in conjugated hyperbilirubinemia. *Drug Metab Dispos* 2014; **42**:561–565.
41 Takamoto T, Hashimoto T, Sano K, Maruyama Y, Inoue K, Ogata S, *et al.* Recovery of liver function after the cessation of preoperative chemotherapy for colorectal liver metastasis. *Ann Surg Oncol* 2010; **17**:2747–2755.
42 Jara M, Bednarsch J, Malinowski M, Pratschke J, Stockmann M. Effects of oxaliplatin-based chemotherapy on liver function: an analysis of impact and functional recovery using the LiMAx test. *Langenbecks Arch Surg* 2016; **401**:33–41.
43 de Graaf W, van Lienden KP, van den Esschert JW, Bennink RJ, van Gulik TM. Increase in future remnant liver function after preoperative portal vein embolization. *Br J Surg* 2011; **98**:825–834.
44 Truant S, Baillet C, Deshorgue AC, El Amrani M, Huglo D, Pruvot FR. Contribution of hepatobiliary scintigraphy in assessing ALPPS most suited timing. *Updates Surg* 2017; **69**:411–419.
45 Schadde E, Raptis DA, Schnitzbauer AA, Ardiles V, Tschuor C, Lesurtel M, *et al.* Prediction of mortality after ALPPS stage-1: an analysis of 320 patients from the International ALPPS Registry. *Ann Surg* 2015; **262**:780–785; (discussion 785–786).
46 Tong YF, Meng N, Chen MQ, Ying HN, Xu M, Lu B, *et al.* Maturity of associating liver partition and portal vein ligation for staged hepatectomy-derived liver regeneration in a rat model. *World J Gastroenterol* 2018; **24**:1107–1119.